CellPress
Partner Journal

Molecular Plant
Research article

Cross-kingdom RNA trafficking from bacteria to fungi enables plant protection against fungal pathogens

Jonatan Niño-Sánchez[1,2,3,4], Huaitong Wu[1,2,4], Rachael Hamby[1,2], Angela Chen[1,2], Min Zhang[1,2], Sandra Mosquera[3] and Hailing Jin[1,2,*]

[1]Department of Microbiology and Plant Pathology, University of California, Riverside, Riverside, CA 92521, USA

[2]Institute for Integrative Genome Biology, University of California, Riverside, Riverside, CA 92521, USA

[3]Department of Plant Production and Forest Resources, Sustainable Forest Management Research Institute (iuFOR), School of Agricultural Engineering, University of Valladolid, 47002 Valladolid, Spain

[4]These authors contributed equally to this article.

***Correspondence: Hailing Jin (hailingj@ucr.edu)**

https://doi.org/10.1016/j.molp.2025.11.003

ABSTRACT

Fungal pathogens pose escalating challenges to global food security, as resistance has emerged against nearly all major fungicides used in agriculture. RNA-based antifungals offer a sustainable and environmentally friendly alternative for disease control, but their deployment is hindered by RNA instability under environmental conditions, especially in soil. In this study, we engineered two plant-beneficial soil bacteria—*Bacillus subtilis* (Gram-positive) and *Pseudomonas putida* (Gram-negative)—to produce double-stranded RNAs (dsRNAs) targeting fungal genes in the foliar and postharvest pathogen *Botrytis cinerea* and the soilborne pathogen *Verticillium dahliae*. We found that both bacterial species secrete RNA through extracellular vesicles (EVs) and that these RNAs are transported into fungal cells, demonstrating cross-kingdom RNA trafficking from bacteria to fungi. Application of dsRNA-containing bacterial EVs to plant leaves suppressed *B. cinerea* infection. In addition, direct treatment with dsRNA-producing bacteria protected both *Arabidopsis thaliana* and tomato plants from infections by *B. cinerea* and *V. dahliae*. Our findings establish beneficial bacteria as a scalable platform for continuous production and delivery of antifungal RNAs, enabling a cost-effective strategy for sustainable crop protection.

Key words: cross-kingdom RNA trafficking, extracellular vesicles, RNA interference, RNAi, RNA-based disease control, microbial communication

Niño-Sánchez J., Wu H., Hamby R., Chen A., Zhang M., Mosquera S., and Jin H. (2026). Cross-kingdom RNA trafficking from bacteria to fungi enables plant protection against fungal pathogens. Mol. Plant. **19**, 100–115.

INTRODUCTION

With continuous global population growth and farmland diminishing, plant scientists and farmers face increasing challenges to produce more food on less land while contending with escalating abiotic and biotic threats to crop health (Delgado-Baquerizo et al., 2020). Among these threats, fungal plant pathogens are particularly devastating, causing substantial crop losses both before and after harvest (Savary et al., 2019). Current management strategies for fungal diseases rely heavily on chemical fungicides, which not only pose risks to environmental and human health (Van de Wouw et al., 2021) but also have driven the widespread emergence of fungicide-resistant pathogen strains. Alarmingly, resistance has been documented for nearly every major fungicide currently used in agriculture and healthcare (Fisher et al., 2018). Developing novel, sustainable, and eco-friendly alternatives is therefore critical to ensure food security, environmental sustainability, and public health.

Recent studies have shown that many fungi can take up RNA, including double-stranded RNA (dsRNA) and small RNAs (sRNAs). The dsRNAs are subsequently processed by the fungal RNA interference (RNAi) machinery into sRNAs capable of silencing complementary fungal mRNAs (Koch et al., 2016; Wang et al., 2016; Qiao et al., 2021). This naturally occurring mechanism enables spray-induced gene silencing (SIGS), a technique that protects plants by applying dsRNAs or sRNAs targeting essential fungal genes (Niu et al., 2021; Mann et al., 2023). SIGS has proven effective against a wide range of fungal pathogens, including *Botrytis cinerea* (Wang et al., 2016; Islam

et al., 2021; Qiao et al., 2021; Niño-Sánchez et al., 2022), *Fusarium graminearum* (Koch et al., 2016), *Sclerotinia sclerotiorum* (McLoughlin et al., 2018; Qiao et al., 2021), *Rhizoctonia solani* (Qiao et al., 2021), *Austropuccinia psidii* (Degnan et al., 2023), and *Phakopsora pachyrhizi* (Hu et al., 2020). Although RNA production has become more affordable due to advances driven by RNA vaccine development, SIGS faces several limitations (Kis et al., 2020). RNAs degrade rapidly in the environment, within 5–7 days on plant surfaces (Niño-Sánchez et al., 2022; Qiao et al., 2023) and in less than 2 days in soil (Dubelman et al., 2014), necessitating frequent reapplication. This makes dsRNA ineffective as an antifungal treatment against soilborne pathogens. In naturally occurring cross-kingdom or cross-species RNA communication between hosts and pathogens, RNA is packaged and protected from environmental degradation inside lipid-enclosed nanoparticles called extracellular vesicles (EVs) (Cai et al., 2018; He et al., 2023; Hamby et al., 2024). In fact, EVs are used by all domains of life to protect and transport secreted RNAs (Hamby et al., 2024). Inspired by this natural mechanism, researchers have employed synthetic nanocarriers such as liposomes (Qiao et al., 2023) and layered-hydroxide clay nanosheets (Mitter et al., 2017; Niño-Sánchez et al., 2022) to enhance RNA stability in SIGS applications. However, these systems still fall short in addressing the major challenges of controlling soilborne pathogens.

Plants coexist with diverse microbial communities in the rhizosphere and on aerial surfaces (Singh et al., 2020). Some microbes promote plant growth and have been exploited as biocontrol agents against plant pathogens (El-Saadony et al., 2022). These beneficial microbes can potentially offer a cost-effective alternative if they could be engineered to consistently produce RNAs *in situ*, on plant tissue or in the soil, replacing the need for external reapplications and potentially enhancing efficacy. Moreover, their intrinsic biocontrol activity may act synergistically with RNA-mediated gene silencing.

In this study, we employed two plant-beneficial bacteria, the Gram-positive *Bacillus subtilis* and the Gram-negative *Pseudomonas putida*, to produce fungal-gene-targeting dsRNAs. We show that both species can be engineered to express antifungal RNAs to protect *Arabidopsis* and tomato plants from two major fungal pathogens: the foliar and postharvest pathogen *B. cinerea* and the soilborne pathogen *Verticillium dahliae*. Furthermore, we demonstrate that both bacteria secrete these RNAs in EVs and that these bacterial EVs (BEVs; referred to as Bs-EVs for *B. subtilis* and Pp-EVs for *P. putida*) could protect both *Arabidopsis* and tomato leaves from *B. cinerea* infection. Our findings establish engineered bacteria as a robust platform for RNA production and delivery, expanding the applicability and practicality of RNAi-based disease management strategies.

RESULTS

B. subtilis can be engineered to produce antifungal RNAs and secrete them in EVs

To produce fungal-gene-targeting RNAs, we selected biocontrol beneficial bacteria, Gram-positive *B. subtilis* and Gram-negative *P. putida.* These species are known for being environmentally friendly, promoting plant growth, and enhancing plant immune responses. We first obtained a strain of *B. subtilis* BG322 (*ΔrncS*) (Herskovitz and Bechhofer, 2000), which lacks RNase III activity and therefore can accumulate long dsRNAs. We generated a BG322 strain, BG322-BcVDS, which expresses a fusion dsRNA targeting the non-conserved regions of three vesicle-trafficking genes, Vacuolar protein sorting-associated protein 51 (*VPS51*), Dynactin subunit 1 (*DCTN1*), and Phosphatidylinositol-3-phosphatase SAC1 (*SAC1*) (VDS), all of which are natural fungal targets of cross-kingdom transferred plant endogenous sRNAs (Cai et al., 2018). This dsRNA has previously shown effectiveness in silencing pathogen genes and reducing virulence (Niño-Sánchez et al., 2022; Qiao et al., 2023). Northern blot analysis confirmed the presence of VDS RNA in BG322-BcVDS compared to the BG322 strain (Figure 1A), and strand-specific RT-PCR further demonstrated that both sense and antisense strands of RNA were present in the purified Bs-EVs (Supplemental Figure 1A).

Since *B. subtilis* is known for producing large amounts of EVs, we investigated whether these RNAs are secreted in Bs-EVs. EVs have been identified as vehicles of RNA protection and transport in all kingdoms of life, including plants, mammals, insects, protists, fungi, archaea, and bacteria (Buck et al., 2014; Koeppen et al., 2016; Cai et al., 2018; Cui et al., 2019; Halder et al., 2021; He et al., 2023; Hamby et al., 2024; Mills et al., 2024). We hypothesized that *B. subtilis* may also be secreting dsRNA within their Bs-EVs. To test this, Bs-EVs were isolated by ultracentrifugation following established protocols (Brown et al., 2014). Abundant VDS RNAs were observed in purified Bs-EVs using northern blot analysis (Figure 1A). Next, to confirm that our BEV isolation procedure successfully yielded intact vesicles, we performed transmission electron microscopy (TEM) imaging and observed structures consistent with the expected EV morphology (Figure 1B). Nanoparticle tracking analysis (NTA) confirmed a peak size of ∼100–110 nm (Supplemental Figure 1B).

To examine whether the engineered RNAs are indeed associated with Bs-EVs, we generated bacterial strains expressing single- and double-stranded *VDS* RNA fused to the optimized fluorescent RNA aptamer Three-Way Junction–4 × Broccoli (3WJ-4×Bro) (BG322-ssVDS-Broccoli and BG322-dsVDS-Broccoli) (Filonov et al., 2014; Bai et al., 2020; Wang et al., 2024). A schematic representation of the dsRNA and ssRNA-3WJ-4×Bro constructs used is provided in Supplemental Figure 1C. Confocal laser scanning microscopy (CLSM) showed that Broccoli, ssVDS-Broccoli, and dsVDS-Broccoli signals all can colocalize with FM4-64-stained membranous vesicles in purified Bc-EV fractions (Figure 1C), providing direct evidence of RNA association with EVs. This result suggests that RNAs expressed in engineered bacteria are secreted in EVs in a sequence-independent manner, which is ideal for broad applications in controlling different pathogens. Further, treatment with micrococcal nuclease (MNase) with and without Triton X-100, which disrupts vesicle membranes (Supplemental Figure 1D), revealed that RNAs were protected within Bs-EVs and accessible to MNase only after membrane disruption (Figure 1D). We also generated BG322 strains expressing dsRNAs targeting *B. cinerea* sRNA biogenesis genes *Dicer-like protein 1* and 2 (*DCL1/2*) (BG322-BcDCL1/2), which also secrete *DCL1/2* dsRNAs in EVs (Supplemental Figure 1E).

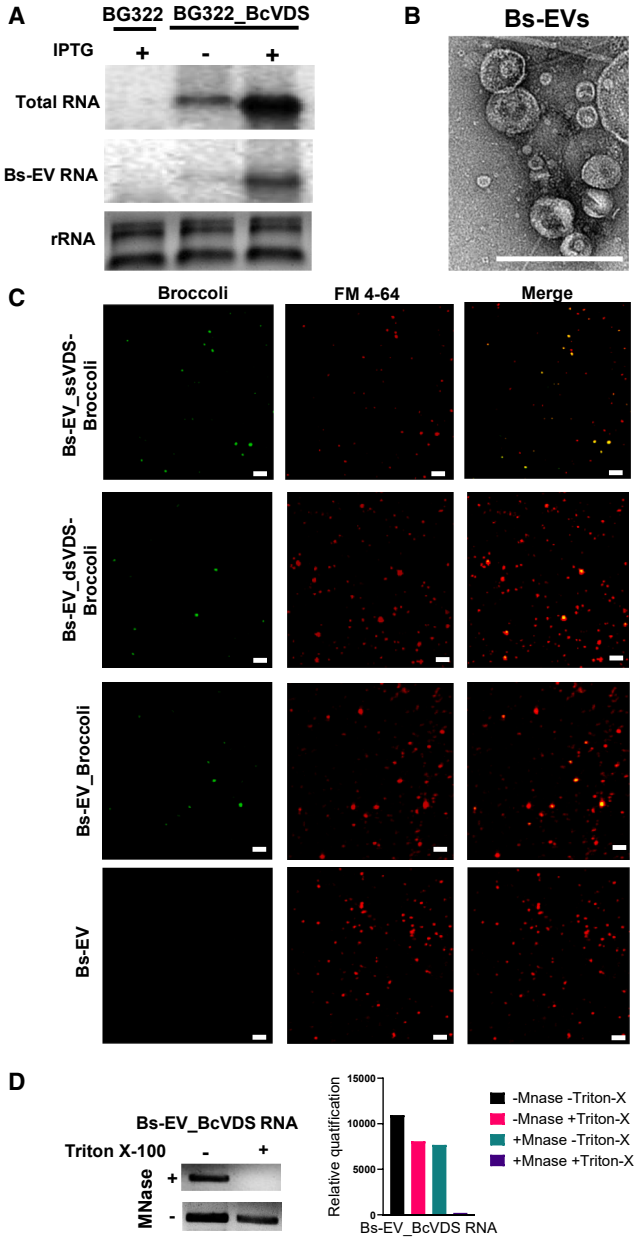

Figure 1. *B. subtilis* produces and secretes antifungal dsRNA within Bs-EVs.

(A) Northern blot showing the presence of the fusion dsRNA targeting *VPS51*, *DCTN1*, *SAC1* in *Botrytis cinerea* (VDS/BcVDS) in both total RNA and purified *Bacillus* extracellular vesicles (Bs-EVs) from the *B. subtilis* BG322 strain expressing BcVDS (BG322-BcVDS). The *B. subtilis* BG322 strain (BG322) without dsRNA construct served as a negative control.

(B) TEM image of purified Bs-EVs isolated from BG322 strains. Scale bar: 200 nm.

(C) CLSM images of Bs-EVs purified from BG322 expressing single-strand VDS-3WJ-4×Broccoli fusion RNA (BG322-ssVDS-Broccoli), BG322 expressing double-strand VDS-3WJ-4×Broccoli fusion RNA (dsVDS-Broccoli), and BG322 expressing 3WJ-4×Broccoli RNA (BG322-Broccoli), showing colocalization of VDS-3WJ-4×Broccoli RNA signal with N-(3-triethylammoniumpropyl)-4-(6-(4-(diethylamino) phenyl)hexatrienyl) pyridinium dibromide (FM4-64) membrane staining, indicating association of RNA with vesicular membranes. Scale bars: 1 μm.

(D) RT-PCR results for VDS RNA in Bs-EVs treated with micrococcal nuclease (MNase), with or without Triton X-100. RNA was protected from degradation unless vesicle membranes were disrupted by Triton X-100, confirming encapsulation of RNA within Bs-EVs.

To determine whether bacterial growth and Bs-EV production are altered by rncS deletion, BG322 (ΔrncS) was examined as compared to the wild-type *B. subtilis* 168. NTA showed that Bs-EV production was not much altered across these strains (Supplemental Figure 1B), although a slight growth delay was observed in BG322 (ΔrncS) (Supplemental Figure 1F).

Bs-EVs mediate cross-kingdom RNA trafficking from bacteria to fungi

To identify a suitable marker for analyzing and visualizing Bs-EVs, we generated a strain expressing YFP-tagged glycine betaine ABC transporter OpuAC (BG322-OpuAC-YFP). We selected OpuAC as a biomarker based on a proteomic study of *B. subtilis* strain 168, which demonstrated that OpuAC is specifically enriched in Bs-EVs with high relative abundance compared to cellular fractions (Brown et al., 2014). Moreover, OpuAC is a well-characterized ABC transporter component, making it a robust and reliable marker for tracking EVs. Indeed, more than 50% of isolated Bs-EVs were labeled with YFP (Figure 2A), indicating that OpuAC is a good marker for Bs-EVs.

We also performed sucrose density gradient fraction to further purify the collected Bs-EVs. Through RT-PCR and immunoblotting, we observed that both the Bs-EV marker OpuAC and the produced RNAs were concentrated between the sucrose gradient fractions, with densities ranging from 1.10 to 1.21 g/ml, which corresponds to the typical density range of exosomes or exosome-like EVs in mammalian, plant, fungal, and bacterial samples (Yuana et al., 2014; He et al., 2021, 2023; De Langhe et al., 2024) (Figure 2B). This provides additional evidence that bacterial cells secrete RNA in EVs.

We next sought to determine whether these Bs-EVs could be internalized by fungi as a mechanism for RNA delivery. We incubated germinated *B. cinerea* spores with BG322-OpuAC-YFP suspension cells or with purified Bs-EVs isolated from BG322-OpuAC-YFP and observed internalization of the fluorescent signal inside fungal cells (Figure 2C). To confirm that RNA was being cotransported into fungal cells with the Bs-EVs, we coincubated BG322-ssVDS-Broccoli and BG322-dsVDS-Broccoli cells with germinated fungal spores. We detected VDS-Broccoli signals inside fungal cells (Figure 2D), indicating successful cross-kingdom RNA delivery. The dsVDS-Broccoli signals were weaker than the VDS-Broccoli likely due to dsRNAs being rapidly processed by the fungal RNAi machinery after uptake, largely diminishing fluorescence. Taken together, these results demonstrate that fungal cells can take up RNAs originating from bacteria via EVs.

Antifungal dsRNA-containing Bs-EVs protect plants from *B. cinerea* infection

After determining that bacteria secrete RNA in Bs-EVs, and that these vesicles can be internalized by fungal cells, we hypothesized that dsRNA-containing Bs-EVs could inhibit fungal

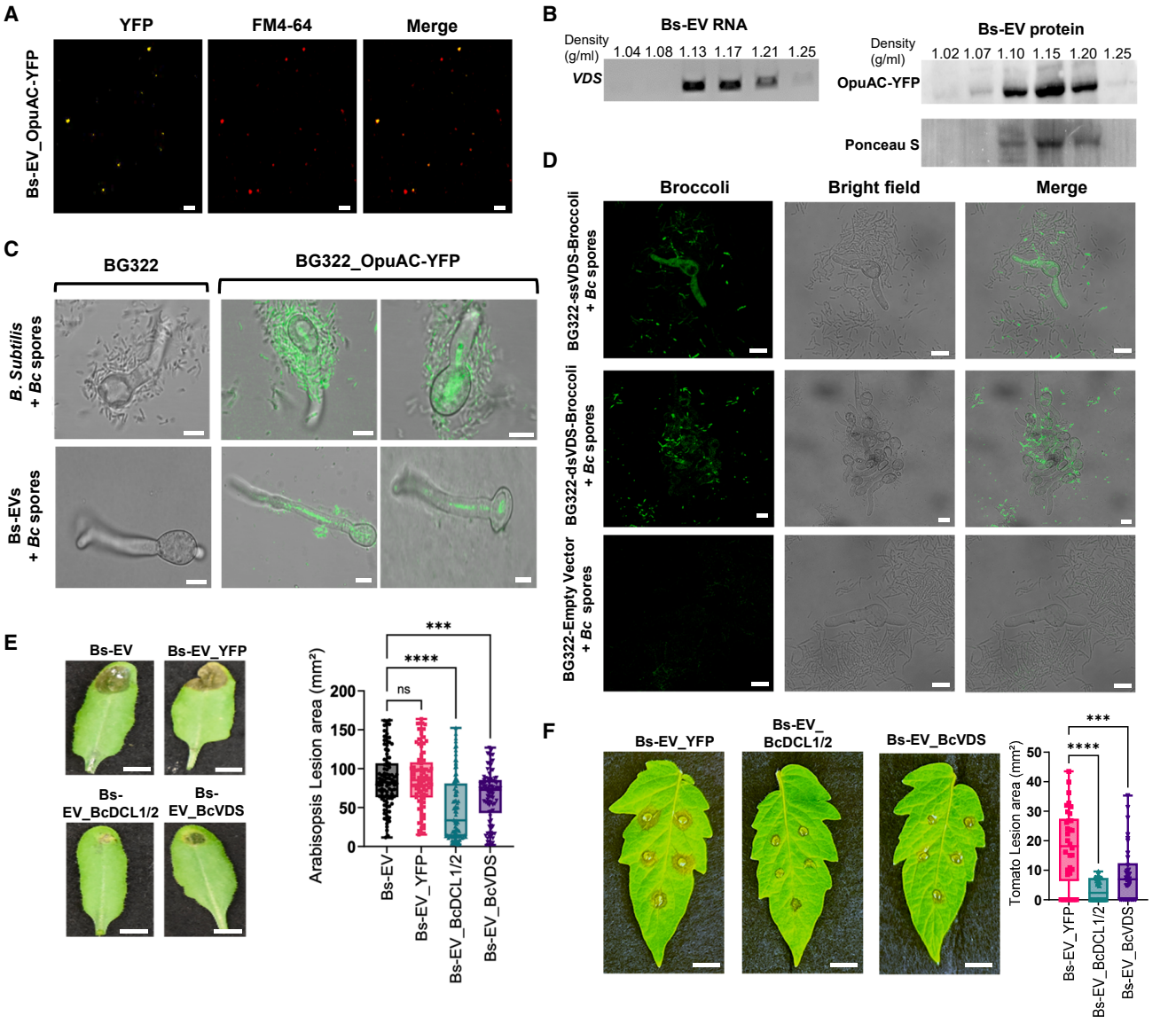

Figure 2. *B. subtilis* Bs-EVs mediate cross-kingdom RNA trafficking from bacteria to fungi and confer antifungal protection.

(A) CLSM showing that the Bs-EV membrane marker OpuAC-YFP colocalizes with FM4-64-stained vesicles in purified Bs-EV fractions. Scale bars: 1 μm.

(B) RT-PCR and immunoblot analyses of sucrose density gradient fractions from Bs-EV of BG322 expressing OpuAC-YFP (BG322-OpuAC-YFP), revealing cofractionation of VDS RNA and the OpuAC-YFP marker in fractions with expected EV density.

(C) CLSM images showing internalization of OpuAC-YFP signal in *B. cinerea* cells after treatment with either BG322-OpuAC-YFP cells or their purified Bs-EVs. Scale bars: 7.5 μm.

(D) Fluorescent RNA signal detected inside *B. cinerea* cells following coincubation with BG322-ssVDS-Broccoli and BG322-dsVDS-Broccoli, indicating uptake of RNA from bacteria. The empty vector strain was used as control. Scale bars: 10 μm.

(E) Lesion area on *A. thaliana* leaves infected with *B. cinerea* is significantly reduced following treatment with Bs-EVs isolated from BG322-BcVDS or BG322 expressing BcDCL1/2 (BG322-BcDCL1/2). Scale bars: 5 mm.

(F) Similar reduction in disease symptoms observed in tomato leaves treated with Bs-EVs from BG322-BcVDS or BG322-BcDCL1/2 before *B. cinerea* infection. Scale bars: 10 mm.

In **(E)** and **(F)**, pictures were taken at 3 dpi. Statistical significance was determined by one-way ANOVA followed by Dunnett's test; ***$p < 0.001$ and ****$p < 0.0001$.

infection. To test this, we isolated Bs-EVs from *Bacillus* strains and treated *Arabidopsis* leaves prior to inoculation with *B. cinerea*. Leaves were maintained in humid conditions after infection, and lesion areas were assessed after 2–3 days. A clear reduction in disease lesion size was observed in leaves treated with Bs-EVs derived from either BG322-BcDCL1/2 or BG322-BcVDS strains (Figure 2E). Interestingly, Bs-EVs isolated from non-induced cultures (without isopropyl-β-D-1-thiogalactopyranoside [IPTG]) also provided noticeable protection, although to a lesser extent than the induced conditions (Supplemental Figure 2A and 2B), suggesting residual dsRNA expression and packaging, consistent with the signal observed in Figure 1A.

To evaluate the efficacy of this strategy in a crop plant, we performed the assay on tomato leaves and again observed significant inhibition of fungal infection (Figure 2F). Treatment with either BG322-BcDCL1/2 or BG322-BcVDS Bs-EVs led to a significant reduction in fungal biomass, as shown in Supplemental Figure 2C. These results indicate that antifungal dsRNA delivered by Bs-EVs is effective not only in reducing visible disease symptoms but also in limiting foliar fungal colonization.

In addition, we analyzed the expression of two plant defense-related genes, PR1 and PR3, in *Arabidopsis* leaves treated with Bs-EVs. We observed a clear induction of both genes within the first 48 h posttreatment (Supplemental Figure 2D), suggesting that Bs-EVs may also trigger plant immune responses, potentially contributing to the observed protection.

To confirm the mechanism of action, we analyzed the expression levels of the targeted fungal genes. Both BcDCL1/2- and BcVDS-derived Bs-EVs led to a clear reduction in the expression of their corresponding target genes in *B. cinerea* in infected tissues from the assays described above (Supplemental Figure 2E). These results confirm that the antifungal effect is mediated through sequence-specific gene silencing triggered by the delivered dsRNAs.

Antifungal dsRNA-producing bacteria protect plants from *B. cinerea* infection

Though we found Bs-EVs to be an effective treatment, EV isolation can be time consuming and costly. In commercial or field settings, direct bacterial application may be more practical and cost effective. To assess the possibility, we repeated the experiments, but instead of treating plant leaves with purified Bs-EVs, we sprayed them with cell suspensions of BG322-BcDCL1/2, BG322-BcVDS, or BG322-YFP strains. In both *Arabidopsis* (Figure 3A) and tomato (Figure 3B), leaves treated with BG322-BcDCL1/2 or BG322-BcVDS exhibited a clear reduction in lesion size.

In addition to symptom reduction, fungal biomass quantification confirmed a significant decrease in colonization levels (Supplemental Figure 3A). Moreover, RT-qPCR analysis of infected tissues showed a marked downregulation of the fungal target genes in treatments with dsRNA-producing strains (Supplemental Figure 3B). Notably, bacterial treatments performed without IPTG induction also provided a low level of protection, although the effects were consistently much lower than in IPTG-induced conditions, indicating that some basal expression of dsRNA occurs even without induction (Supplemental Figure 3C and 3D). We further performed RT-qPCR analysis on IPTG-induced and non-induced BG322 strains and observed an approximately 10-fold increase in dsRNA expression upon IPTG induction (Supplemental Figure 3E). These results demonstrate that direct application of BG322-derived antifungal strains can effectively limit foliar fungal infection through dsRNA-mediated gene silencing.

To explore whether this protective effect depends on EV-mediated RNA delivery, we tested the effect after application of imipramine, a tricyclic antidepressant known to inhibit acid sphingomyelinase, an enzyme critical for ceramide production and EV formation in mammalian cells (Bianco et al., 2009; Catalano and O'Driscoll, 2020). In *B. subtilis* strain BG322, 25 μM imipramine substantially decreased the quantity of secreted Bs-EVs, as confirmed by CLSM (Figure 3C) and NTA, which revealed significant loss of particle quantities, in particular, the 100–200 nm Bs-EV fraction (Figure 3D). This reduction was comparable to that observed in wild-type strain 168 under the same conditions (Supplemental Figure 4A). This shows that imipramine can effectively reduce the amount of secreted EVs in *B. subtilis*. Importantly, imipramine does not affect the growth of *B. subtilis* strains (Supplemental Figure 4B), and imipramine treatment alone did not alter the susceptibility of *Arabidopsis* leaves to *B. cinerea* infection (Supplemental Figure 4C).

However, when imipramine was applied during the growth of BG322-dsRNA strains, their protective effect against *B. cinerea* was abolished, leading to significantly larger lesions (Figure 3E). This loss of disease control highlights the essential role of Bs-EVs in delivering functional dsRNAs and enabling cross-kingdom RNAi.

Antifungal dsRNA-producing *B. subtilis* protects plants from *V. dahliae* infection

While the previous experiments demonstrated the effectiveness of RNA-producing *B. subtilis* in controlling foliar fungal disease, an important objective was to adapt this strategy against soilborne fungal pathogens. To this end, we selected the aggressive soilborne pathogen *V. dahliae* for testing and generated the BG322-VdDCL1/2 strain accordingly. Inspired by previous studies in which *V. dahliae* spores were directly treated with dsRNA (Wang et al., 2016), we coincubated *V. dahliae* spores with BG322-VdDCL1/2 bacterial cells prior to infecting 10-day-old *A. thaliana* seedlings by root-dip inoculation. At 21 days post-inoculation (dpi), this treatment resulted in significantly reduced disease index and fungal biomass (Supplemental Figure 5A and 5B).

To explore a more agronomically relevant application, we transitioned to soil treatment, introducing a newly developed strain, BG322_CE-VdDCL1/2, which expresses dsRNA constitutively from the plasmid without requiring IPTG induction. We first tested this approach in *Arabidopsis*, applying 1.25×10^8 colony-forming units (CFU) per plant just before transplanting, followed by a second application at 7 dpi. At 21 dpi, both BG322-VdDCL and BG322_CE-VdDCL1/2 treatments resulted in a strong reduction in disease index and fungal biomass, with the constitutive strain showing the most robust results (Figure 4A and 4B).

Next, we applied the same soil treatment strategy to tomato plants. Using two applications of 1.25×10^8 CFU per plant (before transplanting and again at 7 dpi), we observed a restoration of plant health in BG322-VdDCL1/2- and BG322_CE-VdDCL1/2-treated plants (Figure 4C). Measurements of canopy area and fresh weight confirmed improved growth (Figure 4D and 4E), and fungal biomass was significantly reduced (Supplemental Figure 5C). Consistently, RT-qPCR analysis showed downregulation of fungal DCL gene expression (Supplemental Figure 5D). Reisolation assays from hypocotyl stem sections revealed that

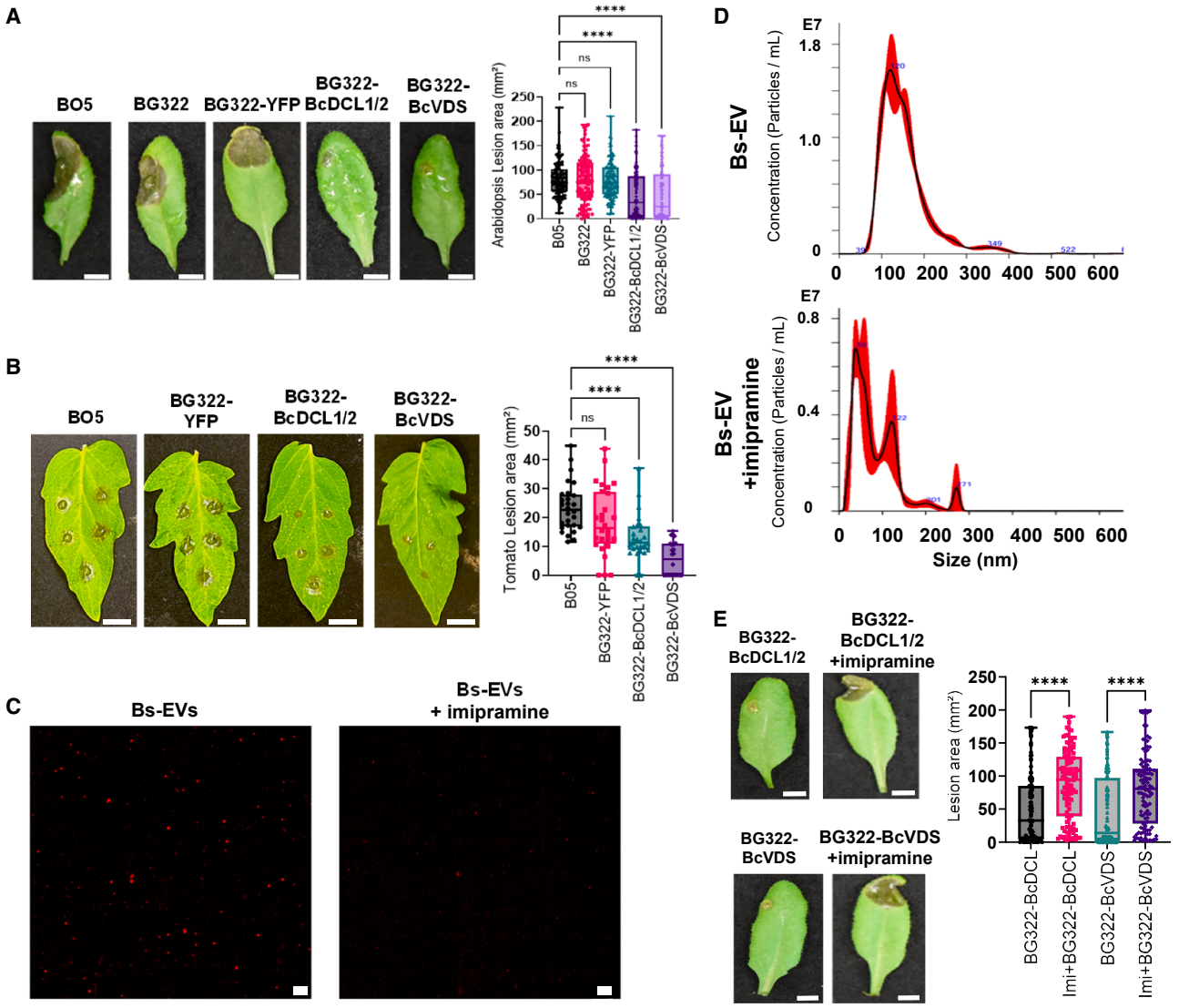

Figure 3. Direct application of dsRNA-producing *B. subtilis* protects plants from *B. cinerea* infection and depends on Bs-EV secretion.

(A) Size of lesions caused by *B. cinerea* infection is significantly reduced in *A. thaliana* leaves treated with BG322-BcVDS or BG322-BcDCL1/2 bacterial suspensions. Scale bars: 5 mm.

(B) Similar disease suppression is observed in tomato leaves treated with dsRNA-producing BG322 strains. Scale bars: 10 mm.

(C) CLSM showing reduced abundance of Bs-EVs in BG322 cultures treated with 25 μM imipramine. Scale bars: 1 μm.

(D) NTA confirms an approximately three-fold decrease in Bs-EV production in imipramine-treated BG322 cultures.

(E) Imipramine treatment abolishes the protective effect of BG322-BcVDS and BG322-BcDCL1/2 against *B. cinerea*, resulting in significantly larger lesions on *A. thaliana* leaves.

In **(A)**, **(B)**, and **(E)**, pictures were taken at 3 dpi. Statistical significance was determined by one-way ANOVA, followed by Tukey's test; ****$p < 0.0001$.

only a small proportion of plants treated with dsRNA-producing strains showed xylem colonization (Supplemental Figure 5E), supporting the observed reductions in fungal colonization and disease symptoms.

To simplify the treatment protocol and enhance its suitability for field applications, we then tested whether a single, higher-dose application could replicate the protective effect. We applied 1.25 × 10^9 CFU per plant (10× the previous dose) as a single pre-infection treatment. This regimen led to disease suppression comparable to the two-dose treatment (Figure 4F), with significant increases in canopy area (Figure 4G) and plant fresh weight (Figure 4H) as well as reductions in fungal biomass (Supplemental Figure 5F) and VdDCL1/2 gene expression (Supplemental Figure 5G). Interestingly, in this high-dose setup, a modest protective effect was also observed in plants treated with non-induced control strains (BG322, BG322-YFP, and BG322-VdDCL1/2 without IPTG) (Figure 4F). This may reflect the known biocontrol activity of *B. subtilis*, even though strain BG322 displays reduced growth compared to its wild-type counterpart 168. Reisolation assays from hypocotyl stem sections confirmed the protective effect of the single high-dose treatment,

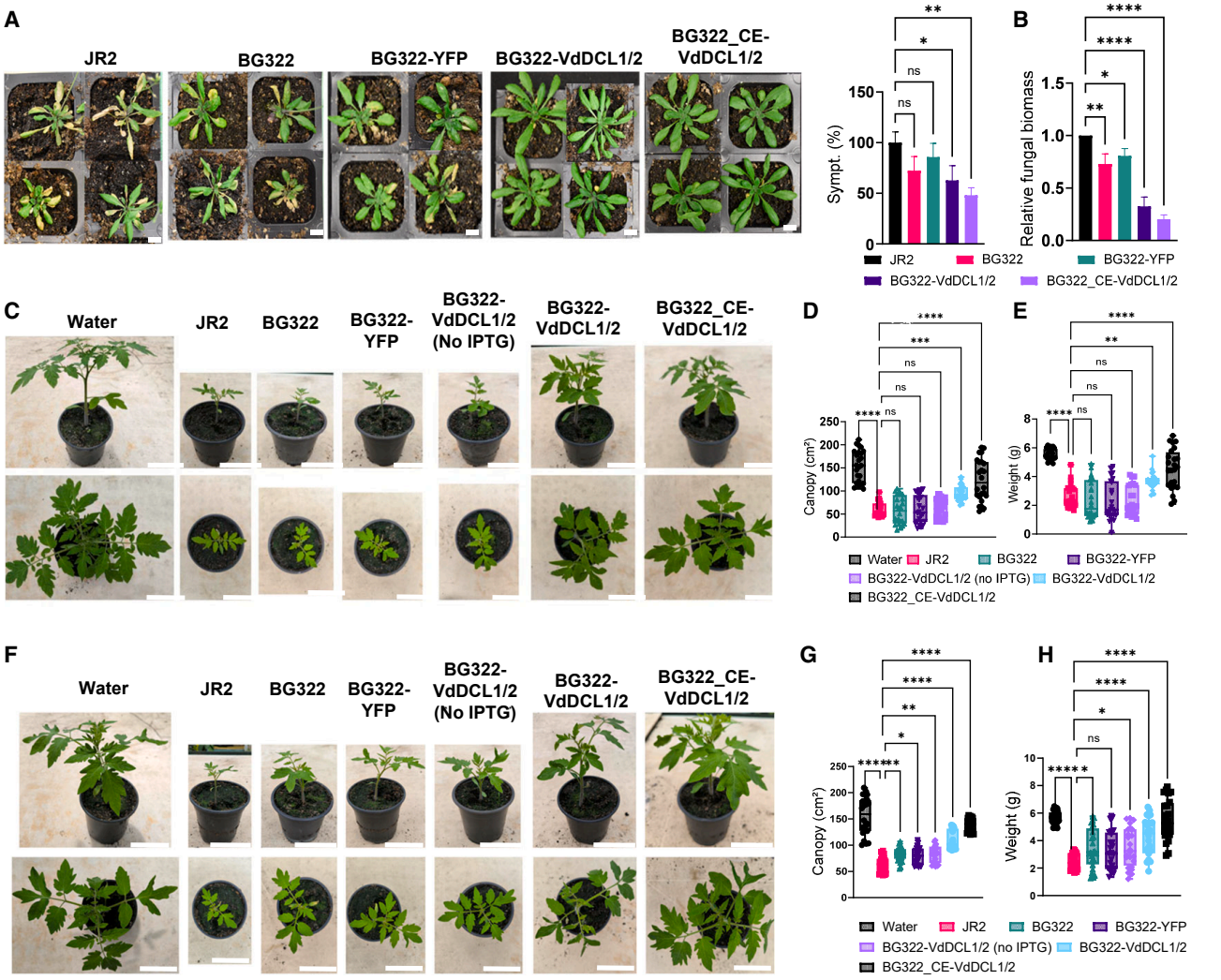

Figure 4. dsRNA-producing *B. subtilis* strains protect *Arabidopsis* and tomato plants from *V. dahliae* infection through root-associated delivery.

(A) Representative images of *A. thaliana* plants at 21 dpi showing reduced disease symptoms after soil treatment with BG322 expressing VdDCL1/2 (BG322-VdDCL1/2) or BG322 constitutively expressing VdDCL1/2 (BG322_CE-VdDCL1/2) (two applications: before transplanting and at 7 dpi). Scale bars: 10 mm.

(B) Quantification of fungal biomass in *Arabidopsis* plants from **(A)**, showing significantly lower levels in dsRNA-treated groups.

(C) Representative images of tomato plants at 21 dpi following the same two-application soil treatment with BG322-VdDCL1/2 or BG322_CE-VdDCL1/2, showing improved plant growth. Scale bars: 10 cm.

(D and E) Measurements of canopy area **(D)** and fresh weight **(E)** of tomato plants from **(C)**, showing restoration of plant growth upon bacterial treatment.

(F) Tomato plants treated with a single high-dose application (1.25×10^9 CFU per plant, i.e., 10× the concentration used in **A** and **C**) of BG322-VdDCL1/2 or BG322_CE-VdDCL1/2 display reduced disease symptoms at 21 dpi. Scale bars: 10 cm.

(G and H) Canopy area **(G)** and fresh weight **(H)** measurements of tomato plants from **(F)**, showing significant recovery following high-dose treatment with dsRNA-producing strains.

In **(B)**, **(D)**, **(E)**, **(G)**, and **(H)**, statistical significance was determined by one-way ANOVA followed by Dunnett's test; $^{*}p < 0.05$, $^{**}p < 0.01$, $^{***}p < 0.001$, and $^{****}p < 0.0001$.

showing a low percentage of plants with detectable *V. dahliae* colonization when treated with VdDCL dsRNA-producing strains (Supplemental Figure 5H).

Across all experiments, the constitutive strain BG322_CE-VdDCL1/2 consistently performed best, achieving the highest levels of protection, the lowest fungal biomass, and minimal fungal reisolation from stem tissues.

P. putida can also produce RNAs and secrete RNA-containing EVs

After confirming that Gram-positive bacteria could be engineered for dsRNA generation and delivery, we next tested whether this approach could also be applied to a Gram-negative bacterium. We selected *P. putida*, a well-known beneficial soil bacterium (Weimer et al., 2020). Following the same rationale as with *B. subtilis*, we used *P. putida* strain KT2440 with an RNase III

mutation (CMA702) (Apura et al., 2021) and generated CMA702 derivatives expressing dsRNAs targeting *B. cinerea* genes *VPS51*, *DCTN1*, and *SAC1* (CMA702-BcVDS), as well as dsRNAs targeting *V. dahliae* genes *DCL1/2* (CMA702-VdDCL1/2). We also generated a control strain, CMA702-YFP, producing a non-specific dsRNA targeting a fluorescent protein sequence, to serve as a negative control in antifungal assays.

We isolated EVs from these engineered strains as described above and performed TEM analysis. The vesicular structures were consistent with BEVs (Figure 5A). In Gram-negative bacteria like *P. putida*, EVs primarily originate from outer membrane blebbing, thus being named outer membrane vesicles, but recent studies have shown that other types, such outer–inner membrane vesicles and explosive outer-membrane vesicles, may also occur (Toyofuku et al., 2019, 2023; De Langhe et al., 2024). To distinguish this complex from those derived from *B. subtilis*, we refer to the vesicles from *P. putida* as Pp-EVs throughout this study.

Using NTA, we confirmed that Pp-EVs displayed the expected size distribution (peak ~100 nm) (Supplemental Figure 6A). To test whether the dsRNA was indeed packaged into these vesicles, we engineered a CMA702 strain expressing *VDS* RNA fused to the 3WJ-4×Broccoli fluorescent RNA aptamer (CMA702-BcVDS-Broccoli). As in *Bacillus*, VDS-3WJ-4×Broccoli was detected in purified Pp-EVs (Supplemental Figure 6B).

To evaluate whether this RNA was enclosed within intact vesicles, we treated purified Pp-EVs with MNase, both in the presence and in the absence of Triton X-100. MNase degraded the RNA only when Triton X-100 was added, confirming that the RNAs are protected within intact Pp-EVs and that Triton X-100 effectively disrupts their membranes (Supplemental Figure 6C and 6D). We also evaluated the growth pattern of CMA702 and its derivative strains and found no obvious difference among RNA-producing CMA702 strains (Supplemental Figure 6E). Others have shown that, compared to wild type *P. putida* KT22440, there is a slight growth delay of CMA702 similar to what we've seen in *B. subtilis* BG322 (Apura et al., 2021).

P. putida Pp-EVs mediate cross-kingdom RNA trafficking from bacteria to fungi

To confirm that *P. putida* Pp-EVs can be internalized by *B. cinerea*, we generated a *P. putida* strain expressing GFP-tagged OprH (CMA702-Oprh-GFP), an outer membrane protein known to be enriched in outer membrane vesicles (Choi et al., 2014). Like Bs-EVs, we also performed density gradient fractionation with Pp-EVs and showed that our expressed RNA and OprH-GFP are present in the same fraction, further showing that the expressed RNA is associated with EVs in *P. putida* (Supplemental Figure 6F). We also evaluated the growth pattern of CMA702 and its derivative strains and found no obvious difference among RNA-producing or OprH-GFP-producing CMA702 strains. Using confocal microscopy, we visualized GFP fluorescence inside fungal cells following incubation with CMA702-OprH-GFP Pp-EVs, indicating vesicle uptake by the fungus (Figure 5B).

Next, we coincubated the CMA702-BcVDS-Broccoli strain with germinated *B. cinerea* spores and observed fluorescent RNA signals within fungal cells. These signals correspond to 3WJ-4×Broccoli aptamer-tagged *VDS* RNA, suggesting that RNA molecules secreted in Pp-EVs are delivered into fungal cells (Figure 5C). Unlike in *B. subtilis* Broccoli-expressing strains, we hardly see any Broccoli signals in *P. putida* Broccoli-expressing strains. This is likely due to the *P. putida* outer membrane being highly selective (Ramos et al., 2015; Löwe et al., 2020), preventing outer membrane penetrance by the DFHBI-1T dye needed for Broccoli signal activation. Together, these observations support the notion that *P. putida*-derived Pp-EVs can mediate cross-kingdom delivery of RNA into fungal pathogens.

Antifungal dsRNA-producing *P. putida* and its secreted EVs protect plants from foliar and root fungal pathogens

To evaluate whether antifungal dsRNA-producing *P. putida* strains could also offer plant protection, we first tested the antifungal potential of Pp-EVs isolated from CMA702-BcVDS and CMA702-BcDCL1/2 strains. *A. thaliana* leaves were treated with the respective Pp-EVs and subsequently inoculated with *B. cinerea*. Lesion size was clearly reduced in both treatments compared to controls (Figure 5D). We performed the same assay in tomato leaves and observed similar disease inhibition (Figure 5D).

Next, to explore a more field-practical approach, we tested whether direct bacterial application could replicate the protective effect. *A. thaliana* and tomato plants were treated with cell suspensions of CMA702-BcVDS or CMA702-BcDCL1/2 prior to *B. cinerea* inoculation. In both species, leaves treated with the dsRNA-producing strains showed a strong reduction in lesion size (Figure 6A). Like *B. subtilis*, we showed that CMA702-BcDCL1/2 without mannitol induction can also exhibit some antifungal effect in *A. thaliana* and tomato against *B. cinerea* (Supplemental Figure 7A and 7B). The fungal biomass reduction and gene silencing effects of CMA702-BcDCL1/2 are shown as well (Supplemental Figure 7C and 7D). Together, these results demonstrate that dsRNA-producing *P. putida* strains can effectively protect plants from foliar fungal pathogens through a cross-kingdom RNAi mechanism, via either purified Pp-EVs or direct bacterial application.

Antifungal dsRNA-producing *P. putida* protects plants from *V. dahliae* infection

To assess whether dsRNA-producing *P. putida* could also provide protection against root-infecting fungal pathogens, we tested the performance of CMA702-VdDCL1/2 in controlling *V. dahliae* in *A. thaliana*. As a preliminary approach, we coapplied bacterial cells with fungal spores during root inoculation, following a strategy like that used for *B. subtilis*. This treatment significantly reduced disease symptoms and fungal biomass (Figure 6B and 6C).

We then evaluated a more practical method for soil application. Soil was treated with CMA702-VdDCL1/2 before fungal inoculation and again at 7 days postinfection. At 21 dpi, *A. thaliana* plants grown in treated soil exhibited markedly improved growth, reduced disease symptoms, and lower fungal biomass (Figure 6D and 6E).

Together with the results obtained using *B. subtilis*, these findings demonstrate that both Gram-positive and Gram-negative beneficial bacteria can be engineered to produce and deliver antifungal

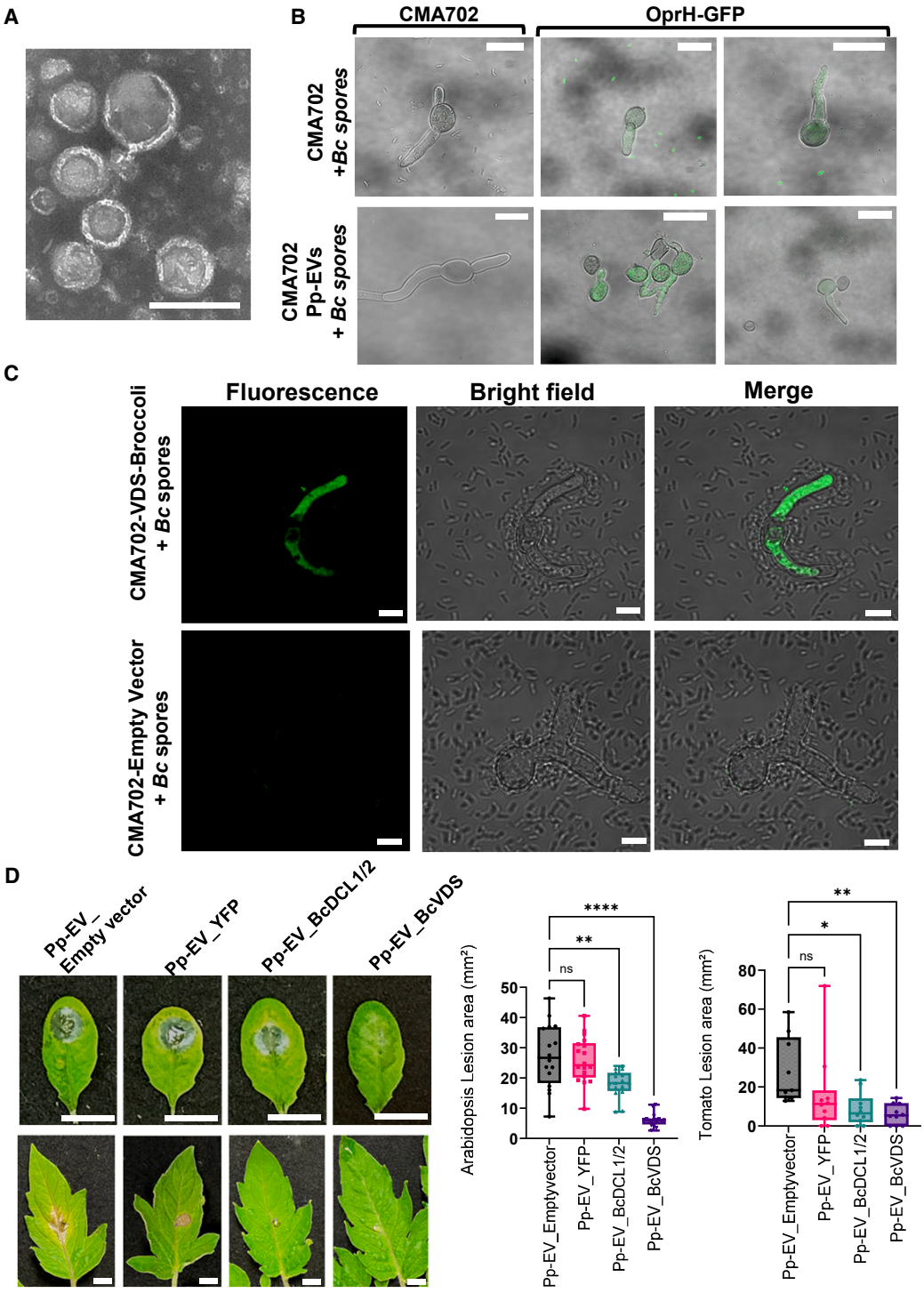

Figure 5. *P. putida* produces and secretes antifungal RNA in Pp-EVs, enabling cross-kingdom delivery and plant protection.

(A) TEM of purified extracellular vesicles from *P. putida* strain CMA702 (CMA702) reveals vesicle structures consistent with bacterial EVs. Scale bar: 200 nm.

(B) CLSM shows internalization of GFP-labeled vesicles into *B. cinerea* cells after incubation with purified *P. putida* extracellular vesicles (Pp-EVs) from CMA702 expressing OprH-GFP (CMA702-OprH-GFP), confirming fungal uptake of EVs. Scale bars: 5 μm.

(C) Fluorescent RNA imaging in *B. cinerea* cells after coincubation with CMA702 expressing BcVDS-3WJ-4×Broccoli (CMA702-BcVDS-Broccoli). The detected signal corresponds to VDS RNA fused to the 3WJ-4×Broccoli aptamer, indicating delivery of vesicle-associated RNA into fungal cells. Scale bars: 5 μm.

(D) Treatment of *A. thaliana* and tomato leaves with Pp-EVs derived from CMA702 expressing BcDCL1/2 (CMA702-BcDCL1/2) or CMA702 expressing BcVDS (CMA702-BcVDS) significantly reduced lesion size following *B. cinerea* infection. Scale bars: 10 mm. Statistical significance was determined by one-way ANOVA followed by Dunnett's test. $^{*}p < 0.05$, $^{**}p < 0.01$, and $^{****}p < 0.0001$.

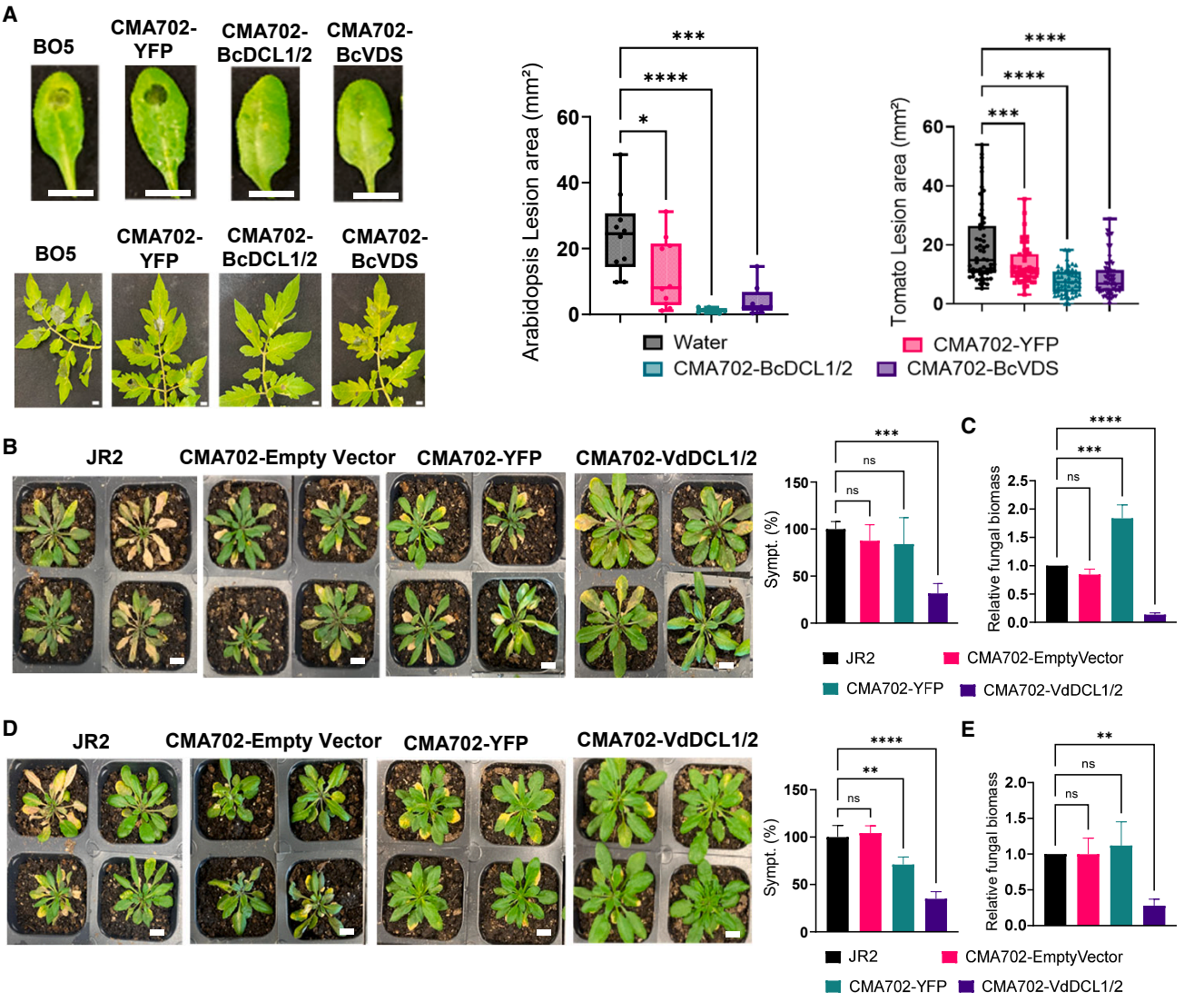

Figure 6. Direct application of dsRNA-producing *P. putida* provides protection against *B. cinerea* and *V. dahliae*.

(A) Lesion size caused by *B. cinerea* was significantly reduced in *A. thaliana* and tomato leaves treated with CMA702-BcDCL1/2 or CMA702-BcVDS bacterial strains. Scale bars: 10 mm.

(B) In A. *thaliana*, coapplication of CMA702-expressing VdDCL1/2 (CMA702-VdDCL1/2) bacterial cells with *V. dahliae* spores during root inoculation significantly reduced disease symptoms. Scale bars: 10 mm.

(C) Quantification of fungal biomass in plants from **(B)** confirmed a reduction in fungal colonization.

(D) In a soil treatment approach, CMA702-VdDCL1/2 was applied before transplanting and again at 7 dpi. Treated *A. thaliana* plants showed improved growth and fewer disease symptoms at 21 dpi. Scale bars: 10 mm.

(E) Fungal biomass in plants from **(D)** confirmed reduced *V. dahliae* colonization following treatment with dsRNA-producing bacteria.

Statistical significance was determined by one-way ANOVA followed by Dunnett's test; $^{*}p < 0.05$, $^{**}p < 0.01$, $^{***}p < 0.001$, and $^{****}p < 0.0001$.

dsRNAs via EVs (Figure 7). This strategy enables effective cross-kingdom RNA delivery and gene silencing in fungal pathogens, offering a versatile and scalable biotechnological platform for crop protection.

DISCUSSION

RNA-based antifungals represent a promising advancement in plant disease management, but their commercial viability remains limited primarily by the instability of RNA in environmental conditions, especially in the rhizosphere. Several nanoparticle-based delivery strategies have been developed to enhance RNA stability in both agricultural and medical contexts. Specifically, lipid-based nanoparticles have been used to package and deliver dsRNA to plant pathogens (Qiao et al., 2023) and to transport therapeutic RNA, drugs, and vaccines in clinical applications (Ahmadzada et al., 2018), including the well-known mRNA COVID-19 vaccines (Thi et al., 2021). In addition, layered-hydroxide nanosheets, known as BioClay, have also been used to stabilize and deliver RNAs to viruses (Mitter et al., 2017), fungal pathogens (Niño-Sánchez et al., 2022), and whiteflies (Jain et al., 2022). Despite these advances, existing nanoparticle-based platforms still face limitations. They do not effectively address the challenges of targeting soilborne pathogens, and they involve relatively high

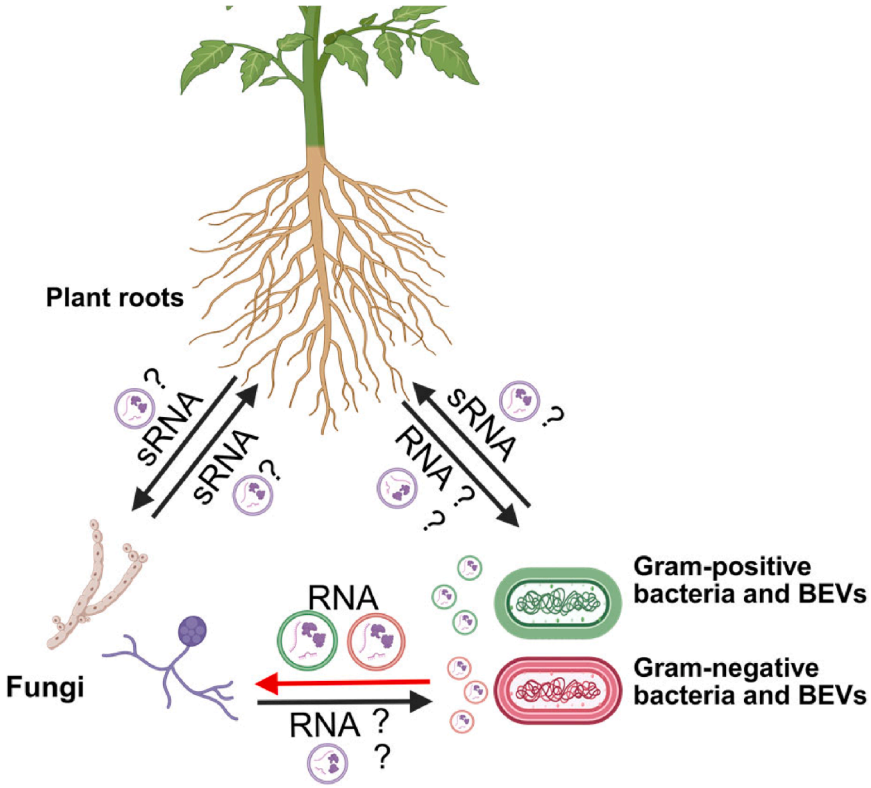

Figure 7. A schematic diagram of plant–fungi–bacteria RNA communications.
Cross-kingdom RNA trafficking may occur among bacteria, fungi, and their plant host in the rhizosphere, regulating gene expression and host–microbe interactions. This study further shows cross-kingdom RNA trafficking and RNAi from bacteria to fungi via bacterial extracellular vesicles. The finding of this research is highlighted in red.

production costs for both RNA and carrier particles, as well as repeated applications in the field.

In this study, we have developed a bacterial platform for dsRNA production and delivery that overcomes these limitations. By using beneficial plant-associated bacteria, *B. subtilis* (Gram-positive) and *P. putida* (Gram-negative), we established a strategy for continuous production and localized delivery of fungal-gene-targeting dsRNAs, either on plant surfaces or within the soil. We showed that these bacteria can secrete dsRNAs via EVs in a somewhat sequence-independent manner and that these RNAs can be taken up by fungal pathogens, leading to effective gene silencing and disease suppression. Our RNA-producing bacterial strains were effective against both foliar (*B. cinerea*) and soilborne (*V. dahliae*) fungal pathogens in two plant systems: the model species *A. thaliana* and the economically important crop tomato. This broad effectiveness greatly enhances the applicability of RNAi-based crop protection strategies, making them more versatile and field relevant.

While a recent study demonstrated RNA trafficking between fungi by using *Trichoderma* to deliver dsRNAs to soilborne fungal pathogens (Wen et al., 2023), our work expands this concept by showing cross-kingdom RNA trafficking from bacteria to fungi. Importantly, we provide mechanistic evidence that the dsRNA is packaged and secreted via BEVs, which mediate delivery into fungal cells. This adds to a growing body of research highlighting the key role of EVs in inter-organismal RNA transport between plants and fungi (Cai et al., 2018; He et al., 2023) and between mammalian hosts and their parasites or pathogens (Buck et al., 2014). Additionally, beyond RNA delivery, some BEVs may carry pathogen-associated molecular patterns virulence factors, or other immunogenic components that can activate immune responses in host organisms, including plants (Rivera et al., 2010; Mancini et al., 2020; McMillan et al., 2021). While the immunomodulatory role of *Bacillus*-derived EVs has not been directly demonstrated in plants, it is plausible that their application could also stimulate plant defense pathways, further contributing to disease protection.

This study presents direct evidence of EV-mediated cross-kingdom RNA transfer from bacteria to fungi, revealing a previously unexplored dimension of cross-kingdom RNA-based communication between microbes within the rhizosphere. This finding supports the hypothesis that bacteria may use endogenous RNAs to influence fungal biology in natural ecosystems. Furthermore, such cross-kingdom RNA exchange and communication may occur naturally in a tripartite manner among bacteria, fungi, and their plant hosts, shaping complex cross-kingdom interactions in the rhizosphere and environment (Figure 7) (Zhang et al., 2016; Ren et al., 2019; Wong-Bajracharya et al., 2022; Silvestri et al., 2025).

Although we demonstrate that EVs can deliver functional RNAs into fungal cells, the exact mechanism of EV and RNA internalization by fungi remains unknown. Based on previous studies in plant and mammalian systems, several possible uptake pathways can be speculated. One likely mechanism is endocytosis, mainly clathrin mediated, a well-characterized route for EV internalization into plant cells. Clathrin-mediated endocytosis involves the formation of clathrin-coated pits and vesicles that internalize membrane-bound cargo, including EVs, through specific adaptor proteins and endocytic machinery (He et al., 2023). Alternatively, EV uptake may occur via clathrin-independent endocytosis pathways, such as those mediated by flotillins or remorin-enriched membrane domains, both of which have been implicated in vesicle trafficking and membrane remodeling (Raffaele et al., 2009; Li et al., 2012). Direct membrane fusion has also been proposed as a potential route for EV entry, particularly in the context of lipid–lipid interactions between vesicles and membranes of destination cells and organisms (Bonsergent et al., 2021). While these hypotheses are supported by studies in other systems, future experiments are needed to elucidate the exact mechanisms operating during bacterial-fungal EV communication.

Our findings establish a new paradigm for microbial cross-kingdom RNA communication, opening exciting avenues for both basic science and sustainable plant disease control.

METHODS

Bacteria strains, culture conditions, and EV isolation

RNase III-deficient bacterial strains *B. subtilis* BG322 and *P. putida* strain CMA702 (KT2440 *Δrnc* derivative) were utilized for dsRNA and BEV production. *B. subtilis* strain BG322 (*ΔrncS SpR*) was kindly provided by Dr. Bechhofer (Mount Sinai School of Medicine of New York University, New York, NY, USA) (Herskovitz and Bechhofer, 2000). *P. putida* strain CMA702 was kindly provided by Dr. Sandra Viegas (Universidade Nova de Lisboa, Lisbon, Portugal) (Apura et al., 2021).

BG322 strains used for plasmid construction were incubated in Luria–Bertani (LB) liquid medium (10 g Bacto Tryptone [Difco Laboratories, Detroit, MI, USA], 10 g NaCl, 5 g Bacto Yeast Extract [Difco Laboratories, Detroit, MI, USA] per liter, adjusted to pH 7.0), and treated with kanamycin (10 mg/ml) when required, at 37°C at 250 rpm. For dsRNA production, BG322 transformants were cultured to reach OD_{600} ~0.8, then IPTG (Sigma-Aldrich, St. Louis, MO, USA) was added to a final concentration of 1.0 mM. Cultures were incubated until reaching the stationary phase (at least 4 h).

CMA702 strains used for plasmid construction were similarly incubated in LB medium with kanamycin (100 mg/ml) at 37°C and 250 rpm. For dsRNA production, CMA702 transformants were grown to OD_{600} ~0.8, followed by addition of D-mannitol to a final concentration of 0.2%. Cultures were then incubated for at least 4 h. All bacterial strains used in this study are listed in Supplemental Table 2.

Bs-EV and Pp-EV isolation was performed with minor modifications to the method previously described by Brown et al. (2014). Briefly, 100 ml of overnight (16 h) bacterial culture was centrifuged for 15 min at 4°C at 4000 *g*. The supernatant was filtered through a 0.22 mm Nalgene Rapid-Flow filter (Thermo Fisher Scientific, Waltham, MA, USA) to remove all remaining cells. Cell removal was confirmed by plating on LB agar, where no colonies formed.

The filtered supernatant was then concentrated using a 100 kDa Amicon ultrafiltration system (Millipore, Burlington, MA, USA), which also removed larger cellular debris and aggregates. The concentrate was eluted in PBS and ultracentrifuged at 174 900 *g* for 90 min at 4°C in a Beckman SW 32 Ti rotor. BEVs were washed twice in 12 ml of PBS and finally resuspended on 300 ml of PBS at 4°C. All the experiments used freshly isolated BEVs.

Plasmid construction

The plasmid pDG148-Stu (Joseph et al., 2001) was modified for dsRNA expression in *B. subtilis* BG322 strain. pDG148-Stu was obtained from the *Bacillus* Genetic Stock Center (Columbus, OH, USA). It is a shuttle vector capable of replicating in *Escherichia coli* HT115(DE3) (via the pBR322 origin) and in *B. subtilis* BG322 (via the pUB110 origin). It was developed for IPTG-inducible expression of a foreign insert cloned into its unique *Stu*I restriction site, downstream of a P*spac* promoter. A 312 bp fragment corresponding to the dsRNA against *VdDCL1* and *VdDCL2* was amplified using the plasmid pHellsgate-Bc+Vd-DCLs (Wang et al., 2016) as template, with the pair of primers StuI-NotI-VdDCL1/2-F and StuI-Pspac-NotI-VdDCL1/2-R (Supplemental Table 1). The fragment was cloned into the pENTR/D-TOPO vector (Thermo Fisher Scientific, Waltham, MA, US) and excised by *Stu*I digestion. Ligation into linearized pDG148-Stu yielded the pDG148+VdDCL1/2 plasmid, capable of expressing *VdDCL1/2* dsRNA in BG322, since the insert was flanked by two P*spac* promoters for IPTG-inducible bidirectional transcription. A *Not*I restriction site was added in between the promoters and the dsRNA insert to facilitate exchange of sequences via *Not*I digestion and ligation. Using this strategy, we generated several constructs: a 490 bp fragment of BcDCL1/2 (from pHellsgate-Bc-DCL1/2; Wang et al., 2016) amplified with NotI-BcDCL1/2-F/R; a 516 bp fragment covering BcVPS51, BcDCTN1, and BcSac1 (from pHellsgate-Bc-VPS51+DCTN1+SAC1 plasmid; Qiao et al., 2021) using NotI-BcVDS-F/R primers; and a 516 bp YFP fragment amplified with NotI-YFP-F/R primers (Supplemental Table 1). The resulting plasmids were pDG148+BcDCL1/2, pDG148+BcVDS, and pDG148+YFP, respectively.

The pDG148+CE-VdDCL1/2 backbone was generated by deleting the *lacI* gene from pDG148+VdDCL1/2 via *Esp*3I digestion, followed by end repair using T4 DNA polymerase (New England Biolabs, Ipswich, MA, USA) and blunt-end ligation with T4 DNA ligase (Thermo Fisher Scientific). Removal of *lacI* eliminates repression of the *lacO* operator in the P*spac* promoter, allowing constitutive (inducer-free) expression (Wen et al., 2023).

For constitutive expression of OpuAC-YFP fusion protein in BG322 (Supplemental Figure 1C), the *OpuAC* coding sequence was amplified from the BG322 genome using EcoRI-StuI-OpuAC-F and BamHI-OpuAC-R primers (Supplemental Table 1), and the *YFP* coding sequence was amplified with EcoRI-BamHI-YFP-F and StuI-YFP-R primers (Supplemental Table 1). The *YFP* fragment was first cloned into pENTR/D-TOPO to generate pENTR-YFP, which was linearized with *EcoR*I and *BamH*I. The *OpuAC* fragment was then inserted to create pENTR-OpuAC-YFP. The *OpuAC-YFP* fusion sequence was excised using *Stu*I and cloned into the backbone vector of pDG148+CE-VdDCL1/2 (after removing the dsRNA cassette and 3′ P*spac* promoter), yielding the final pDG148+CE-OpuAC-YFP plasmid.

To generate the pDG148+VDS3WJ4×Broccoli plasmid, we first constructed pDG148-attR, amplifying the attR region from pEarlyGate 100 using Stu-attR1-F and Stu-attR2-R primers (Supplemental Table 1), followed by ligation into pDG148-Stu. The VDS sequence was amplified with SacII-VDS-F and XmaI-VDS-R (Supplemental Table 1) and cloned into pENTR-MCS-3WJ4×Broccoli, resulting in pENTR-VDS3WJ4×Broccoli.

The plasmid pJOE771.1 (Hoffmann and Altenbuchner, 2015) was modified for dsRNA expression in *P. putida* strain CMA702 (KT2440 *Δrnc* derivative). An *EcoR*I restriction site was inserted between the pMtlE promoters and the dsRNA insert site, allowing easy replacement of the insert by *EcoR*I digestion and ligation. Primers used for cloning the *P. putida* constructs are listed in Supplemental Table 1.

Growth curve measurement

Overnight bacterial cultures were diluted to an initial OD_{600} of 0.1 in LB medium and incubated in Erlenmeyer flasks at 150 rpm (37°C for *B. subtilis* and 30°C for *P. putida*). OD_{600} readings were taken at specific time points. For samples exceeding OD_{600} >1.2, a 10-fold dilution was performed and values were adjusted accordingly.

TEM analysis

Purified EVs were analyzed by negative staining. A 5 μl aliquot was applied to Formvar-carbon-coated copper grids (3.0 mm, EMS) for 1 min, blotted, and stained twice with 1% uranyl acetate (30 s and 2 min). Grids were air dried and visualized using a Talos L120 transmission electron microscope at 120 kV.

NTA

EV size distribution and concentration were measured using a NanoSight NS300 with a 405 nm laser and NTA software v.3.1 (Malvern Panalytical). Samples were diluted 20×–100× in 0.22-μm-filtered PBS and analyzed at a flow rate of 50 units. For each sample, four 60-s videos were recorded and analyzed.

Triton X-100 and MNase treatment

To assess RNA protection within vesicles, 0.5% Triton X-100 was added to EV preparations and incubated on ice for 30 min to disrupt membranes. Subsequently, 2000 units of MNase (NEB, #M0247S) was added to a 100 μl reaction and incubated at 37°C for 30 min.

Fungal strains and culture conditions

Fungal cultures of *B. cinerea* BO5.10 and *V. dahliae* JR2 were revived from frozen mycelia stocks in 15% (v/v) glycerol at −80°C. *B. cinerea* B05.10 was cultured on malt extract agar consisting of 20 g malt extract, 10 g Bacto proteose peptone (Difco Laboratories, Detroit, MI, USA), and 15 g agar per liter. Plates were incubated for 10 days to promote sporulation. Spores were then harvested and diluted in 1% Saboraud maltose broth for use in inoculation experiments. *V. dahliae* was routinely cultured on PDA medium (24 g potato dextrose broth [Difco Laboratories, Detroit, MI, USA] and 15 g agar per liter). For rapid spore production, *V. dahliae* cultures grown for 3 days in GOX liquid medium (60 g sucrose, 7 g $NaNO_3$, 3 g Bacto Peptone [Difco Laboratories, Detroit, MI, USA], 1 g de KH_2PO_4, 0.5 g de $MgSO_4{\cdot}7H_2O$, 0.5 g KCl per liter adjusted to pH 7.0 with NaOH) at 120 rpm. For inoculations, fungal spores were collected and washed twice by filtration through a double-layered cheesecloth using Milli-Q autoclaved water, followed by centrifugation at 2500 *g* for 15 min. Spores were then resuspended in sterile Milli-Q water to the appropriate concentration.

Pathogenicity test

To evaluate the efficacy of dsRNA-producing bacteria or their associated EVs in preventing fungal infection, plants were pre-treated with bacterial or EV solutions prior to fungal inoculation. For the *B. cinerea* inoculation, *A. thaliana* plant leaves were sprayed with a bacterial suspension of BG322 strains at approximately 5×10^9 CFU/ml (∼0.5 ml per plant) or were treated with 10 μl droplets of purified BEV solutions. When required, IPTG was added to the bacterial suspensions at a final concentration of 0.1 mM. After the bacterial solutions were allowed to dry (∼2 h), three leaves per plant were inoculated with 10 μl drops of a *B. cinerea* spore suspension (10^5 spores/ml). In EV-treated plants, spores were applied directly at the droplet site. Plants were incubated for 3 days at 22°C in a translucent plastic container. Lesion areas were calculated by diameter measurements using an electronic caliper.

For *V. dahliae* inoculation in *A. thaliana*, three bacterial application strategies were tested: (i) coinoculation: a mixture of BG322 bacterial suspension (1.25×10^8 CFU/ml) and fungal spores was applied simultaneously at the time of root-dip inoculation; (ii) two soil applications: soil was treated with 1 ml of BG322 bacterial suspension (1.25×10^8 CFU/ml) 2 h before transplanting the inoculated seedlings, followed by a second 1 ml application at 7 dpi; and (iii) single high-dose soil application: a one-time application of 10× concentrated bacterial suspension (1.25×10^9 CFU/ml) was applied to the soil 2 h before transplanting. For all treatments, 2-week-old *Arabidopsis* plants were uprooted, rinsed in Milli-Q autoclaved water, and dipped for 3 min in a *V. dahliae* spore suspension (10^6 spore/ml). Plants were then transferred to fresh or bacterial-treated soil. Disease progression was assessed at 21 dpi by quantifying the percentage of diseased rosette leaves, following the method of Fradin et al. (2011). For tomato (*Solanum lycopersicum*, cv. Money Maker), inoculations were conducted according to Fradin et al. (2009), with minimal modifications. Briefly, 10-day-old seedlings were uprooted, roots were rinsed with water, and ∼0.5 cm of the root tip was trimmed to standardize infection. Roots were dipped for 5 min in a suspension of *V. dahliae* spores (10^7 spores/ml) and transplanted into soil treated with BG322 strains using either the two-application or the single high-dose protocol described above. After 3 weeks, relative canopy area was quantified using ImageJ software from overhead images, and the fresh weight of each plant was measured. A fungal reisolation assay was also conducted by collecting stem sections just above the cotyledons as described in Fradin et al. (2009). Briefly, sections were surface sterilized (15 min in 70% ethanol, 15 min in 10% sodium hypochlorite, followed by three water rinses), sliced with a sterile scalpel, and plated on PDA medium containing chloramphenicol (34 mg/ml) to assess vascular colonization.

Total RNA extraction and northern blot assay

Leaves from *A. thaliana* plants inoculated with *V. dahliae* were collected and immediately frozen at −80°C. Total RNA was extracted using TRIzol Reagent (Thermo Fisher Scientific, Waltham, MA, USA) according to the manufacturer's instructions. RNA was eluted in DEPC-treated water (Sigma-Aldrich, St. Louis, MO, USA) and treated with DNase I (Thermo Fisher Scientific, Waltham, MA, USA) to eliminate contaminating genomic DNA. RNA quality was assessed by electrophoresis on 1.2% agarose gels, and concentration was measured using a NanoDrop spectrophotometer. The absence of genomic DNA was confirmed by PCR, using primers specific for *A. thaliana* and *V. dahliae* genes.

For RNA extraction from the BEVs the same protocol was used, with the addition of an MNase treatment step prior to RNA purification, following the manufacturer's instructions (Thermo Fisher Scientific, Waltham, MA, USA). This step ensured degradation of external nucleic acids and allowed for selective analysis of RNA enclosed within the vesicles.

Total RNA extracted from BEVs was separated on 1.1% agarose gel containing 1× MOPS and 0.5% formaldehyde. Following electrophoresis, RNA was transferred to a membrane via salt bridge overnight in 20× SSC buffer. The membrane was then baked at 80°C for 2 h to fix the RNA. Hybridization was performed using ^{32}P-labeled probes, and radioactive signals were detected using a Typhoon 9410 phosphorimager (GE Healthcare). XmaI-VDS-R (Supplemental Table 1) was used to probe for VDS RNA.

ImageJ gel band quantification

RT-PCR amplification results of MNase- and Triton-X-treated BEVs were quantified using ImageJ's Analyze Gels function. Lanes were first selected through Analyze > Gels > Select First Lane / Select Next Lane and then plotted through Analyze > Gels > Plot Lanes. The area of the peak shown was measured and plotted.

RT-qPCR for gene expression and fungal biomass quantification and RT-PCR for dsRNA detection in BEVs

After RNA extraction, cDNA was synthesized using the Superscript III First-Strand Synthesis System (Thermo Fisher, Waltham, MA, USA) following the manufacturer's instructions. RT-qPCR was performed using SYBR Green Supermix (Bio-Rad Laboratories, Hercules, CA, USA) in a CFX384 Real-Time PCR System (Bio-Rad) with the following thermal cycling conditions: 95°C for 15 min followed by 40 cycles of 94°C for 30 s, 50°C for 30 s, and 72°C for 30 s. A melt curve analysis was conducted at the end of the run (0.5°C increments every 10 s from 65°C to 95°C) to confirm specificity of amplification.

Fungal biomass in infected samples was estimated by quantifying *V. dahliae* actin transcript levels using Vd-actin 2F and Vd-actin 2R primers (Supplemental Table 1). Data were normalized to *A. thaliana* actin transcript levels (At-actin F and At-actin R) (Supplemental Table 1) using the $2^{-\Delta\Delta Ct}$ method (Livak and Schmittgen, 2001).

To detect dsRNA strands in BEVs, cDNA synthesis was performed using strand-specific primers (SacII-VDS-F and XmaI-VDS-R) with the Superscript III First-Strand Synthesis System (Thermo Fisher, Waltham, MA, USA) following the manufacturer's instructions. RT-PCR was subsequently performed using Phusion High-Fidelity DNA Polymerase (Thermo Fisher, Waltham, MA, USA) following the manufacturer's instructions. PCR products were visualized on 1.2% agarose gels stained with ethidium bromide.

Density gradient fractionation of BEVs

BEVs were also purified using discontinuous sucrose density gradient centrifugation. Sucrose stock solutions (w/v) were prepared at the following concentrations: 10%, 16%, 22%, 28%, 34%, 40%, 46%, 52%, 58%, 64%, 70%, and 90%. A 15 ml ultracentrifuge tube was loaded by carefully layering 1 ml of each sucrose solution sequentially to form the gradient. EV samples were pre-mixed with 1 ml of 10% sucrose and carefully loaded on top of the gradient. Centrifugation was performed in a swinging-bucket rotor at 100 000 *g* for 16 h at 4°C. Following centrifugation, six fractions of 2 ml each were collected from the gradient. Each fraction was transferred to a new ultracentrifuge tube, diluted to 12 ml with PBS, and centrifuged again at 174 900 *g* for 2 h at 4°C. The resulting EV pellets were collected for downstream analyses.

Fungal uptake efficiency

To evaluate the uptake efficiency of EVs by fungal cells, internalization of YFP-labeled Bs-EVs by *B. cinerea* cells was assessed using CLSM, following the protocol described by Hamby et al. (2020). Briefly, YFP-labeled Bs-EVs were isolated from a 100 ml culture and resuspended in 300 ml of PBS. A 10 μl aliquot of the Bs-EV suspension was added to germinated fungal spores placed on a glass microscope slide with 3 ml of PDA medium. The slide was incubated for 3 h at room temperature. To remove non-internalized vesicles, samples were treated with 1% Triton X-100. Imaging was performed using a Leica TCS SP5 confocal laser scanning microscope (Leica Microsystems, Wetzlar, Germany). YFP excitation was achieved using an argon laser at 514 nm, and the fluorescence emission was detected at 515–560 nm.

Visualization of fungal uptake of bacterially expressed RNA

B. subtilis BG322 strains carrying the plasmid pDG148-Stu (empty vector), pDG148-VDS3WJ4×Broccoli, or pDG148-dsVDS3WJ4×BroccoliSDV were cultured and induced with IPTG as described above. Following induction, 0.5 ml of bacterial culture was centrifuged at 5000 *g* for 5 min and the pellet resuspended in 500 μl of YEPD medium containing germinated *B. cinerea* spores. The bacterial–fungal coculture was incubated overnight at room temperature.

To visualize RNA uptake, DFHBI-1T (fluorophore for Broccoli-tagged RNAs) was added at a 1:500 dilution, and the samples were incubated in the dark for 30 min prior to imaging. Fluorescent signal was detected by CLSM using a 488 nm laser as excitation and 500–600 nm as the detection range.

FUNDING

This work was supported by grants from the National Institutes of Health (R35GM136379), the National Science Foundation (IOS 2020731), and the United States Department of Agriculture (2021-67013-34258) to H.J. and the Spanish Ministry of Science, Innovation and Universities (PID2023-148417OAI00) and Junta de Castilla y León (CLU-2025-2-07) to J.N.-S.

ACKNOWLEDGMENTS

We thank Dr. David Bechhofer (Mount Sinai School of Medicine of New York University, New York, NY, USA) for providing the *B. subtilis* strain BG322 and Dr. Sandra Viegas (Universidade Nova de Lisboa, Lisbon, Portugal) for providing the *P. putida* strain CMA702 (KT2440 *Δrnc* derivative). No conflict of interest is declared.

AUTHOR CONTRIBUTIONS

H.J. conceived the idea, oversaw the entire project, supervised the postdocs and PhD students, and edited the manuscript. J.N.-S. and H.W. performed most of the experiments and contributed to conceptualization, data curation and analysis, methodology development, and writing of the manuscript. R.H. contributed to the experiments of plant pathogen assays, methodology development, and writing of the original draft. A.C. contributed to the experiments related to *P. putida*. M.Z. generated most of the TEM and microscopy images, and S.M. contributed to the pathogen assays.

SUPPLEMENTAL INFORMATION

Supplemental information is available at *Molecular Plant Online*.

Received: August 26, 2025
Revised: October 12, 2025
Accepted: November 9, 2025
Published: November 11, 2025

REFERENCES

Ahmadzada, T., Reid, G., and McKenzie, D.R. (2018). Fundamentals of siRNA and miRNA therapeutics and a review of targeted nanoparticle delivery systems in breast cancer. Biophys. Rev. **10**:69–86.

Apura, P., de Lorenzo, V., Arraiano, C.M., Martínez-García, E., and Viegas, S.C. (2021). Ribonucleases control distinct traits of Pseudomonas putida lifestyle. Environ. Microbiol. **23**:174–189.

Bai, J., Luo, Y., Wang, X., Li, S., Luo, M., Yin, M., Zuo, Y., Li, G., Yao, J., Yang, H., et al. (2020). A protein-independent fluorescent RNA aptamer reporter system for plant genetic engineering. Nat. Commun. **11**:3847.

Bianco, F., Perrotta, C., Novellino, L., Francolini, M., Riganti, L., Menna, E., Saglietti, L., Schuchman, E.H., Furlan, R., Clementi, E., et al. (2009). Acid sphingomyelinase activity triggers microparticle release from glial cells. EMBO J. **28**:1043–1054.

Bonsergent, E., Grisard, E., Buchrieser, J., Schwartz, O., Théry, C., and Lavieu, G. (2021). Quantitative characterization of extracellular vesicle uptake and content delivery within mammalian cells. Nat. Commun. **12**:1864.

Brown, L., Kessler, A., Cabezas-Sanchez, P., Luque-Garcia, J.L., and Casadevall, A. (2014). Extracellular vesicles produced by the Gram-positive bacterium Bacillus subtilis are disrupted by the lipopeptide surfactin: Vesicle production and disruption inBacillus subtilis. Mol. Microbiol. **93**:183–198.

Buck, A.H., Coakley, G., Simbari, F., McSorley, H.J., Quintana, J.F., Le Bihan, T., Kumar, S., Abreu-Goodger, C., Lear, M., Harcus, Y., et al. (2014). Exosomes secreted by nematode parasites transfer small RNAs to mammalian cells and modulate innate immunity. Nat. Commun. **5**:5488.

Cai, Q., Qiao, L., Wang, M., He, B., Lin, F.-M., Palmquist, J., Huang, S.-D., and Jin, H. (2018). Plants send small RNAs in extracellular vesicles to fungal pathogen to silence virulence genes. Science **360**:1126–1129.

Catalano, M., and O'Driscoll, L. (2020). Inhibiting extracellular vesicles formation and release: a review of EV inhibitors. J. Extracell. Vesicles **9**:1703244.

Choi, C.-W., Park, E.C., Yun, S.H., Lee, S.-Y., Lee, Y.G., Hong, Y., Park, K.R., Kim, S.-H., Kim, G.-H., and Kim, S.I. (2014). Proteomic characterization of the outer membrane vesicle of Pseudomonas putida KT2440. J. Proteome Res. **13**:4298–4309.

Cui, C., Wang, Y., Liu, J., Zhao, J., Sun, P., and Wang, S. (2019). A fungal pathogen deploys a small silencing RNA that attenuates mosquito immunity and facilitates infection. Nat. Commun. **10**:4298.

De Langhe, N., Van Dorpe, S., Guilbert, N., Vander Cruyssen, A., Roux, Q., Deville, S., Dedeyne, S., Tummers, P., Denys, H., Vandekerckhove, L., et al. (2024). Mapping bacterial extracellular vesicle research: insights, best practices and knowledge gaps. Nat. Commun. **15**:9410.

Degnan, R.M., Shuey, L.S., Radford-Smith, J., Gardiner, D.M., Carroll, B.J., Mitter, N., McTaggart, A.R., and Sawyer, A. (2023).

Double-stranded RNA prevents and cures infection by rust fungi. Commun. Biol. **6**:1234.

Delgado-Baquerizo, M., Guerra, C.A., Cano-Díaz, C., Egidi, E., Wang, J.-T., Eisenhauer, N., Singh, B.K., and Maestre, F.T. (2020). The proportion of soil-borne pathogens increases with warming at the global scale. Nat. Clim. Chang. **10**:550–554.

Dubelman, S., Fischer, J., Zapata, F., Huizinga, K., Jiang, C., Uffman, J., Levine, S., and Carson, D. (2014). Environmental fate of double-stranded RNA in agricultural soils. PLoS One **9**:e93155.

El-Saadony, M.T., Saad, A.M., Soliman, S.M., Salem, H.M., Ahmed, A. I., Mahmood, M., El-Tahan, A.M., Ebrahim, A.A.M., Abd El-Mageed, T.A., Negm, S.H., et al. (2022). Plant growth-promoting microorganisms as biocontrol agents of plant diseases: Mechanisms, challenges and future perspectives. Front. Plant Sci. **13**:923880.

Filonov, G.S., Moon, J.D., Svensen, N., and Jaffrey, S.R. (2014). Broccoli: rapid selection of an RNA mimic of green fluorescent protein by fluorescence-based selection and directed evolution. J. Am. Chem. Soc. **136**:16299–16308.

Fisher, M.C., Hawkins, N.J., Sanglard, D., and Gurr, S.J. (2018). Worldwide emergence of resistance to antifungal drugs challenges human health and food security. Science **360**:739–742.

Fradin, E.F., Zhang, Z., Juarez Ayala, J.C., Castroverde, C.D.M., Nazar, R.N., Robb, J., Liu, C.-M., and Thomma, B.P.H.J. (2009). Genetic dissection of Verticillium wilt resistance mediated by tomato Ve1. Plant Physiol. **150**:320–332.

Fradin, E.F., Abd-El-Haliem, A., Masini, L., van den Berg, G.C.M., Joosten, M.H.A.J., and Thomma, B.P.H.J. (2011). Interfamily transfer of tomato Ve1 mediates Verticillium resistance in Arabidopsis. Plant Physiol. **156**:2255–2265.

Halder, L.D., Babych, S., Palme, D.I., Mansouri-Ghahnavieh, E., Ivanov, L., Ashonibare, V., Langenhorst, D., Prusty, B., Rambach, G., Wich, M., et al. (2021). Candida albicans induces cross-kingdom miRNA trafficking in human monocytes to promote fungal growth. mBio **13**:e0356321.

Hamby, R., Wang, M., Qiao, L., and Jin, H. (2020). Synthesizing fluorescently labeled dsRNAs and sRNAs to visualize fungal RNA uptake. Methods Mol. Biol. **2166**:215–225.

Hamby, R., Cai, Q., and Jin, H. (2025). RNA communication between organisms inspires innovative eco-friendly strategies for disease control. Nat. Rev. Mol. Cell Biol. **26**:81–82. https://doi.org/10.1038/s41580-024-00807-y.

He, B., Cai, Q., Qiao, L., Huang, C.-Y., Wang, S., Miao, W., Ha, T., Wang, Y., and Jin, H. (2021). RNA-binding proteins contribute to small RNA loading in plant extracellular vesicles. Nat. Plants **7**:342–352.

He, B., Wang, H., Liu, G., Chen, A., Calvo, A., Cai, Q., and Jin, H. (2023). Fungal small RNAs ride in extracellular vesicles to enter plant cells through clathrin-mediated endocytosis. Nat. Commun. **14**:4383.

Herskovitz, M.A., and Bechhofer, D.H. (2000). Endoribonuclease RNase III is essential in Bacillus subtilis: Bs-RNase III is essential in B. subtilis. Mol. Microbiol. **38**:1027–1033.

Hoffmann, J., and Altenbuchner, J. (2015). Functional characterization of the mannitol promoter of Pseudomonas fluorescens DSM 50106 and its application for a mannitol-inducible expression system for Pseudomonas putida KT2440. PLoS One **10**:e0133248.

Hu, D., Chen, Z.-Y., Zhang, C., and Ganiger, M. (2020). Reduction of Phakopsora pachyrhizi infection on soybean through host- and spray-induced gene silencing. Mol. Plant Pathol. **21**:794–807.

Islam, M.T., Davis, Z., Chen, L., Englaender, J., Zomorodi, S., Frank, J., Bartlett, K., Somers, E., Carballo, S.M., Kester, M., et al. (2021). Minicell-based fungal RNAi delivery for sustainable crop protection. Microb. Biotechnol. **14**:1847–1856.

Jain, R.G., Fletcher, S.J., Manzie, N., Robinson, K.E., Li, P., Lu, E., Brosnan, C.A., Xu, Z.P., and Mitter, N. (2022). Foliar application of clay-delivered RNA interference for whitefly control. Nat. Plants **8**:535–548.

Joseph, P., Fantino, J.-R., Herbaud, M.-L., and Denizot, F. (2001). Rapid orientated cloning in a shuttle vector allowing modulated gene expression inBacillus subtilis. FEMS Microbiol. Lett. **205**:91–97.

Kis, Z., Kontoravdi, C., Shattock, R., and Shah, N. (2020). Resources, production scales and time required for producing RNA vaccines for the global pandemic demand. Vaccines (Basel) **9**:3.

Koch, A., Biedenkopf, D., Furch, A., Weber, L., Rossbach, O., Abdellatef, E., Linicus, L., Johannsmeier, J., Jelonek, L., Goesmann, A., et al. (2016). An RNAi-based control of Fusarium graminearum infections through spraying of long dsRNAs involves a plant passage and is controlled by the fungal silencing machinery. PLoS Pathog. **12**:e1005901.

Koeppen, K., Hampton, T.H., Jarek, M., Scharfe, M., Gerber, S.A., Mielcarz, D.W., Demers, E.G., Dolben, E.L., Hammond, J.H., Hogan, D.A., and Stanton, B.A. (2016). A novel mechanism of host-pathogen interaction through sRNA in bacterial outer membrane vesicles. PLoS Pathog. **12**:e1005672.

Li, R., Liu, P., Wan, Y., Chen, T., Wang, Q., Mettbach, U., Baluska, F., Samaj, J., Fang, X., Lucas, W.J., and Lin, J. (2012). A membrane microdomain-associated protein, Arabidopsis Flot1, is involved in a clathrin-independent endocytic pathway and is required for seedling development. Plant Cell **24**:2105–2122.

Livak, K.J., and Schmittgen, T.D. (2001). Analysis of relative gene expression data using real-time quantitative PCR and the 2(-Delta Delta C(T)) Method. Methods **25**:402–408.

Löwe, H., Sinner, P., Kremling, A., and Pflüger-Grau, K. (2020). Engineering sucrose metabolism in Pseudomonas putida highlights the importance of porins. Microb. Biotechnol. **13**:97–106.

Mancini, F., Rossi, O., Necchi, F., and Micoli, F. (2020). OMV vaccines and the role of TLR agonists in immune response. Int. J. Mol. Sci. **21**:4416.

Mann, C.W.G., Sawyer, A., Gardiner, D.M., Mitter, N., Carroll, B.J., and Eamens, A.L. (2023). RNA-based control of fungal pathogens in plants. Int. J. Mol. Sci. **24**:12391.

McLoughlin, A.G., Wytinck, N., Walker, P.L., Girard, I.J., Rashid, K.Y., de Kievit, T., Fernando, W.G.D., Whyard, S., and Belmonte, M.F. (2018). Identification and application of exogenous dsRNA confers plant protection against Sclerotinia sclerotiorum and Botrytis cinerea. Sci. Rep. **8**:7320.

McMillan, H.M., Zebell, S.G., Ristaino, J.B., Dong, X., and Kuehn, M.J. (2021). Protective plant immune responses are elicited by bacterial outer membrane vesicles. Cell Rep. **34**:108645.

Mills, J., Gebhard, L.J., Schubotz, F., Shevchenko, A., Speth, D.R., Liao, Y., Duggin, I.G., Marchfelder, A., and Erdmann, S. (2024). Extracellular vesicle formation in Euryarchaeota is driven by a small GTPase. Proc. Natl. Acad. Sci. USA **121**:e2311321121.

Mitter, N., Worrall, E.A., Robinson, K.E., Li, P., Jain, R.G., Taochy, C., Fletcher, S.J., Carroll, B.J., Lu, G.Q.M., and Xu, Z.P. (2017). Clay nanosheets for topical delivery of RNAi for sustained protection against plant viruses. Nat. Plants **3**:16207.

Niño-Sánchez, J., Sambasivam, P.T., Sawyer, A., Hamby, R., Chen, A., Czislowski, E., Li, P., Manzie, N., Gardiner, D.M., Ford, R., et al. (2022). BioClay™ prolongs RNA interference-mediated crop protection against Botrytis cinerea. J. Integr. Plant Biol. **64**:2187–2198.

Niu, D., Hamby, R., Sanchez, J.N., Cai, Q., Yan, Q., and Jin, H. (2021). RNAs - a new frontier in crop protection. Curr. Opin. Biotechnol. **70**:204–212.

Qiao, L., Lan, C., Capriotti, L., Ah-Fong, A., Nino Sanchez, J., Hamby, R., Heller, J., Zhao, H., Glass, N.L., Judelson, H.S., et al. (2021). Spray-induced gene silencing for disease control is dependent on the efficiency of pathogen RNA uptake. Plant Biotechnol. J. **19**:1756–1768.

Qiao, L., Niño-Sánchez, J., Hamby, R., Capriotti, L., Chen, A., Mezzetti, B., and Jin, H. (2023). Artificial nanovesicles for dsRNA delivery in spray-induced gene silencing for crop protection. Plant Biotechnol. J. **21**:854–865.

Raffaele, S., Bayer, E., Lafarge, D., Cluzet, S., German Retana, S., Boubekeur, T., Leborgne-Castel, N., Carde, J.-P., Lherminier, J., Noirot, E., et al. (2009). Remorin, a solanaceae protein resident in membrane rafts and plasmodesmata, impairs potato virus X movement. Plant Cell **21**:1541–1555.

Ramos, J.-L., Sol Cuenca, M., Molina-Santiago, C., Segura, A., Duque, E., Gómez-García, M.R., Udaondo, Z., and Roca, A. (2015). Mechanisms of solvent resistance mediated by interplay of cellular factors in Pseudomonas putida. FEMS Microbiol. Rev. **39**:555–566.

Ren, B., Wang, X., Duan, J., and Ma, J. (2019). Rhizobial tRNA-derived small RNAs are signal molecules regulating plant nodulation. Science **365**:919–922.

Rivera, J., Cordero, R.J.B., Nakouzi, A.S., Frases, S., Nicola, A., and Casadevall, A. (2010). Bacillus anthracis produces membrane-derived vesicles containing biologically active toxins. Proc. Natl. Acad. Sci. USA **107**:19002–19007.

Savary, S., Willocquet, L., Pethybridge, S.J., Esker, P., McRoberts, N., and Nelson, A. (2019). The global burden of pathogens and pests on major food crops. Nat. Ecol. Evol. **3**:430–439.

Silvestri, A., Ledford, W.C., Fiorilli, V., Votta, C., Scerna, A., Tucconi, J., Mocchetti, A., Grasso, G., Balestrini, R., Jin, H., et al. (2025). A fungal sRNA silences a host plant transcription factor to promote arbuscular mycorrhizal symbiosis. New Phytol. **246**:924–935.

Singh, B.K., Trivedi, P., Egidi, E., Macdonald, C.A., and Delgado-Baquerizo, M. (2021). Author Correction: Crop microbiome and sustainable agriculture. Nat. Rev. Microbiol. **19**:72.

Thi, T.T.H., Suys, E.J.A., Lee, J.S., Nguyen, D.H., Park, K.D., and Truong, N.P. (2021). Lipid-based nanoparticles in the clinic and clinical trials: From cancer nanomedicine to COVID-19 vaccines. Vaccines (Basel) **9**:359.

Toyofuku, M., Nomura, N., and Eberl, L. (2019). Types and origins of bacterial membrane vesicles. Nat. Rev. Microbiol. **17**:13–24.

Toyofuku, M., Schild, S., Kaparakis-Liaskos, M., and Eberl, L. (2023). Composition and functions of bacterial membrane vesicles. Nat. Rev. Microbiol. **21**:415–430.

Van de Wouw, A.P., Scanlan, J.L., Marcroft, S.J., Smith, A.J., Sheedy, E.M., Perndt, N.W., Harrison, C.E., Forsyth, L.M., and Idnurm, A. (2021). Fungicide sensitivity and resistance in the blackleg fungus, Leptosphaeria maculans, across canola growing regions in Australia. Crop Pasture Sci. **72**:994–1007.

Wang, M., Weiberg, A., Lin, F.-M., Thomma, B.P.H.J., Huang, H.-D., and Jin, H. (2016). Bidirectional cross-kingdom RNAi and fungal uptake of external RNAs confer plant protection. Nat. Plants **2**:16151.

Wang, S., He, B., Wu, H., Cai, Q., Ramírez-Sánchez, O., Abreu-Goodger, C., Birch, P.R.J., and Jin, H. (2024). Plant mRNAs move into a fungal pathogen via extracellular vesicles to reduce infection. Cell Host Microbe **32**:93–105.e6.

Weimer, A., Kohlstedt, M., Volke, D.C., Nikel, P.I., and Wittmann, C. (2020). Industrial biotechnology of Pseudomonas putida: advances and prospects. Appl. Microbiol. Biotechnol. **104**:7745–7766.

Wen, H.-G., Zhao, J.-H., Zhang, B.-S., Gao, F., Wu, X.-M., Yan, Y.-S., Zhang, J., and Guo, H.-S. (2023). Microbe-induced gene silencing boosts crop protection against soil-borne fungal pathogens. Nat. Plants **9**:1409–1418.

Wong-Bajracharya, J., Singan, V.R., Monti, R., Plett, K.L., Ng, V., Grigoriev, I.V., Martin, F.M., Anderson, I.C., and Plett, J.M. (2022). The ectomycorrhizal fungus Pisolithus microcarpus encodes a microRNA involved in cross-kingdom gene silencing during symbiosis. Proc. Natl. Acad. Sci. USA **119**:e2103527119.

Yuana, Y., Levels, J., Grootemaat, A., Sturk, A., and Nieuwland, R. (2014). Co-isolation of extracellular vesicles and high-density lipoproteins using density gradient ultracentrifugation. J. Extracell. Vesicles **3**:23262.

Zhang, T., Zhao, Y.-L., Zhao, J.-H., Wang, S., Jin, Y., Chen, Z.-Q., Fang, Y.-Y., Hua, C.-L., Ding, S.-W., and Guo, H.-S. (2016). Cotton plants export microRNAs to inhibit virulence gene expression in a fungal pathogen. Nat. Plants **2**:16153.